

Two Measure is Two Know: Calibration-free Full Duplex Monitoring for Software Radio Platforms

Jie Wang

Washington University in St. Louis
jie.w@wustl.edu

Jonathan Gornet

Washington University in St. Louis
jonathan.gornet@wustl.edu

Alex Orange

University of Utah
alex.orange@utah.edu

Leigh Stoller

University of Utah
stoller@flux.utah.edu

Gary Wong

University of Utah
gtw@flux.utah.edu

Jacobus Van Der Merwe

University of Utah
kobus@cs.utah.edu

Sneha Kumar Kasera

University of Utah
kasera@cs.utah.edu

Neal Patwari

Washington University in St. Louis
npatwari@wustl.edu

ABSTRACT

Future virtualized radio access network (vRAN) infrastructure providers (and today’s experimental wireless testbed providers) may be simultaneously uncertain what signals are being transmitted by their base stations and legally responsible for their violations. These providers must monitor the spectrum of transmissions and external signals without access to the radio itself. In this paper, we propose FDMonitor, a full-duplex monitoring system attached between a transmitter and its antenna to achieve this goal. Measuring the signal at this point on the RF path is necessary but insufficient since the antenna is a bidirectional device. FDMonitor thus uses a bidirectional coupler, a two-channel receiver, and a new source separation algorithm to simultaneously estimate the transmitted signal and the signal incident on the antenna. Rather than requiring an offline calibration, we also adaptively estimate the linear model for the system on the fly. FDMonitor has been running on a real-world open wireless testbed, monitoring 19 SDR platforms controlled (with bare metal access) by outside experimenters over a seven month period, sending alerts whenever a violation is observed. Our experimental results show that FDMonitor accurately separates signals across a range of signal parameters. Over more than 7 months of observation, it achieves a positive predictive value of 97%, with a total of 20 false alerts.

1 INTRODUCTION

Demand for spectrum and flexibility has led to technology trends that make radio access networks (RAN) increasingly dynamic and software driven. Spectrum sharing systems [36], e.g., the citizens broadband radio service (CBRS) [26], require a RAN to dynamically change frequency bands to coexist with multiple different types of wireless systems.

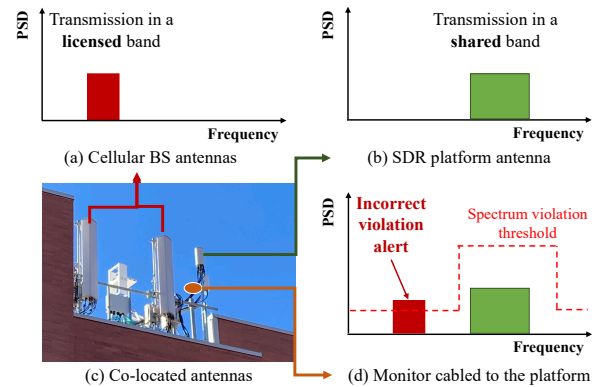


Figure 1: A co-located base station’s signal is incident to an SDR platform’s antenna. If the monitor cannot separate the two signals, it may believe that its own SDR’s transmitted signal is violating spectrum rules, which would be a false alarm.

Infrastructure sharing systems, as proposed in emerging virtualized RAN (vRAN) architectures [31, 38, 43, 54], provide the flexibility needed to efficiently meet the needs of multiple heterogeneous service providers. As another example, radio dynamic zones (RDZs) are also likely to use dynamic and spectrum-agile approaches to provide services from a shared infrastructure, and thus require spectrum monitoring technologies [23]. These architectures promise to increase the efficiency of spectrum and infrastructure utilization.

However, flexibility and dynamism increase the complexity of the enforcement of spectrum regulation. It is unclear how spectrum sharing systems will identify and handle spectrum violations. For virtualized RANs, an infrastructure provider (InP) [43] can possibly lease a software-defined base

station (BS) to a service provider (SP) who might cause a spectrum violation. In this case, it seems likely that InPs would continue to be legally responsible for spectrum violations as they are today [19]. Violations may be intentional [52] or unintentional, caused by erroneous configuration changes, a software bug, or even malware. Since the transmitted signal spectrum is an interaction between software and analog hardware (power amplifiers, filters, etc.) it is not straightforward to identify problems solely in software. Furthermore, it is advantageous to operate a monitor independent from the BS radio that is leased to a SP.

While these monitoring problems might seem far in the future, there is a strong need to address these *today* in existing wireless experimental testbeds [1–4, 6] that are openly available to researchers. Users of these testbeds run real-world next-generation wireless experiments with bare-metal access to compute and SDR resources, and thus can transmit with a wide range of frequencies, modulations, and bandwidths. Users are asked to follow spectrum regulations, but fundamentally, the testbed operator is liable, and must shut down transmitters in violation [25]. In this paper, we design and build FDMonitor, a robust system to reliably conduct this monitoring.

One real-world spectrum violation that we’ve observed with FDMonitor is when platform users set the gain on the power amplifier too high, in an attempt to maximize the transmit power. Doing so can cause severe harmonics induced by the nonlinearities of the power amplifier. Although the user may be unaware, their high power harmonics can violate out-of-band power limits, and interfere with other licensed users. Being the source of interference can harm relationships with other (licensed) wireless operators. We periodically receive inquiries asking if we caused the interference seen by some other licensed operator, and FDMonitor measurements have been critical to demonstrate that our platform was not the cause.

FDMonitor allows testbed operators to meet two critical requirements:

- User monitoring: observe transmissions from its SDR platforms and detect any spectrum violation to ensure compliance. For transmission in shared bands, this requires simultaneously monitoring other users’ signals (from external sources).
- Spectrum protection: monitor the environmental use of spectrum to observe (to be able to act against) interference sources.

We present a full-duplex monitoring system (FDMonitor) [60] to achieve simultaneous spectrum monitoring of both the environment and the transmissions by the platform. FDMonitor continuously estimates the signal transmitted by the platform user and external signals. Very importantly,

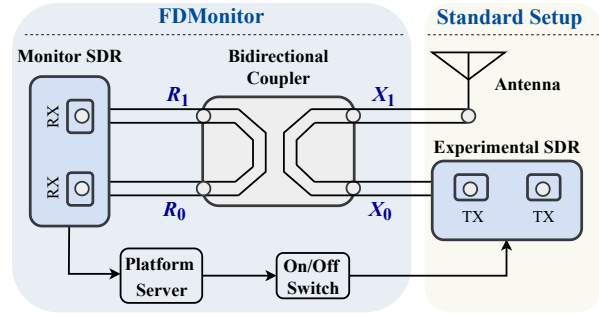


Figure 2: Architecture of FDMonitor, the proposed full-duplex monitoring system

FDMonitor addresses a significant challenge that is posed by co-located antennas, as shown in Figure 1. Consider an SDR platform’s antenna deployed on a cellular tower (where platform antennas are deployed to test cellular technologies): although a user is transmitting in an authorized band, an antenna used by a cellular provider *CP* might transmit at 50 W on the same tower¹. Since an antenna is a two-way device, some of *CP*’s signal, although many dB less than transmitted, impinges on the platform’s antenna. If we directly cable a monitor to the platform, it records both transmitted and incident signals, and cannot distinguish them. *In this case the monitor wrongly concludes that the user is transmitting in the band owned by CP and, for spectrum compliance, aborts the user’s operation.*

Hardware design of FDMonitor. The design of FDMonitor addresses the problem that antennas both emit (most of) the platform’s transmit signal and receive signals from external co-channel sources. As shown in Figure 2, we use a bidirectional coupler to measure the forward and backward traveling signals on the RF path, in two *different* linear combinations, which we call R_0 and R_1 . Here, R_0 receives more of the signal from the platform transmitter than R_1 , whereas, R_1 receives more of the incident signal than R_0 .

Unfortunately, R_0 and R_1 are misleading estimates of the actual transmitted signal (denoted by X_0) and the incident signal (denoted by X_1), respectively. The challenge is that a wideband bidirectional coupler does not perfectly isolate these two signals — the overall system can provide only 10–15 dB difference in the power of one source between the two coupled outputs. This is because RF subsystems are not perfectly matched over the wide bandwidths across which frequency-agile SDR platforms must be able to operate. Counterintuitively, the platform’s transmitted signal and the incident signal are carried in *both* directions on the RF chain, so a *directional* coupler can only do so much.

¹Towers and rooftop antenna locations are typically owned by an InP who leases tower space to multiple wireless operators.

Source Separation in FDMonitor. Separating the two signals (transmitted and incident), without knowing anything about either signal, becomes our significant problem. An insight we use is that the transmitted signal should be independent of the signal incident to the antenna, and further, most digital communication signals are non-Gaussian. This insight allows us to apply blind source separation algorithms like independent component analysis (ICA) to separate the transmit and incident signals. However, ICA results in scaling and permutation ambiguities. Our source separation algorithm uses the mixing matrix inverse to recover the scale, which gives us accurate signal power levels. Correlation coefficients [8] and the maximum power of the coupler’s two receiver chains are used in the algorithm to correctly identify the two estimates as “transmitted” or “incident”.

We implement FDMonitor and deploy it on 19 SDRs available to researchers on an open wireless research testbed, and thoroughly evaluate its performance with different RF settings (carrier frequency, bandwidth, transmit power and signal type) to verify that FDMonitor operates correctly. FDMonitor has been running continuously for over 7 months on the testbed, alerting administrators of any spectrum violation, who may then turn off the user’s transmitter. We investigate each violation and find that FDMonitor has achieved a 97% positive predictive value over this 7 month period.

2 RELATED WORK

Full-duplex monitoring of the shared SDR platforms is at the intersection of relevant research on (i) vRAN, (ii) full-duplex communication, and (iii) spectrum sensing.

2.1 Virtual RAN

Next-generation virtual RAN architectures are rapidly evolving. We describe vRAN here to address its novel needs for spectrum monitoring.

vRAN Architecture. In a conventional distributed RAN (D-RAN), every BS is composed of a baseband unit (BBU) and remote radio heads (RRHs), all located at the same cell site [33]. RRHs interface with the antenna on one end, and the BBU via fiber on the other. RRHs have radio frequency (RF) capabilities like power amplification and sampling, whereas BBUs host baseband functions for further processing.

In comparison to D-RAN, vRAN’s main idea is network function virtualization (NFV) in which network functions are decoupled from the physical hardware [46]. BBUs of all BSs, based on NFV principles, are not only centralized, but also virtualized as a cloud. They are deployed on the same commodity server hardware and can be created dynamically when changes are needed over frequency, time and space [38]. RRHs, instead, remain at the cell towers yet support flexible functions via SDR hardware.

The Business Model of vRAN. Multiple roles are needed in vRAN. Different business models map these roles with actual entities [27, 40, 41, 43]. Roles and functions include:

- *Infrastructure providers (InPs)* deploy and own the physical infrastructure including RAN, fronthaul/backhaul transport, core networks and etc. BSs are provided to SPs as a service by splitting them into slices. InPs are required to detect and disable spectrum violations.
- *Virtual network providers (VNP)s* can operate on licensed or unlicensed spectrum and create virtual network resources for SPs to use. VNPs may or may not own spectrum resources.
- *Service providers (SPs)* lease BSs from InP(s) and virtualized network resources from VNPs. In doing so, they can provide services to their subscribers.

Experimental Wireless Testbeds. Experimental wireless testbeds can be seen as an abstraction of a vRAN today. The testbed providers are the InPs responsible for managing the deployed infrastructure and detecting spectrum violations. The VNPs, include various entities, such as spectrum access system (SAS) operators for the CBRS band [30] or mobile network operators for cellular bands [43]. Researchers are the SPs requesting shareable physical and network slices for testing new wireless technologies.

Recent wireless infrastructures include: (i) POWDER, COSMOS and AERPAW testbeds [18, 45, 53] as part of the U.S. NSF’s platforms for advanced wireless research (PAWR) program [6]; (ii) 5G-VINNI, 5G-EVE and 5GENESIS [7] as 5G testbeds being developed by joint efforts across Europe; (iii) Bristol Is Open in the UK [34] and ADRENALINE [47] in Spain for exploring 5G, software defined networking and large-scale Internet of things (IoT) techniques.

2.2 Full-duplex Communication

Full-duplex communication [42, 44, 56, 63] enables simultaneous transmission and reception in the same channel. It requires neither time division duplexing (TDD) or frequency division duplexing (FDD) and thus significantly increases spectral efficiency and network capacity [10]. Both full-duplex monitoring and full-duplex communication allow co-channel signal differentiation, but the former is focused on monitoring spectrum use, while the latter is for bidirectional communication. Self-interference (SI) [11], i.e., the contamination of the received signal with the transmitted signal, is the biggest challenge for both. Proposed SI cancellation methods can be classified as: (i) propagation-domain, (ii) analog-domain, and (iii) digital-domain.

Propagation-domain SI cancellation methods isolate the transmit and receive chain carefully for electromagnetically suppressing the SI before it shows up in the analog circuitry [56], via path loss enhancement [42], cross-polarization [12], transmit beamforming [55], or a circulator [16].

Analog-domain SI cancellation methods subtract a copy of the transmitted signal from received signals in the analog receive chain [56]. The methods can be classified as non-adaptive [28] and adaptive [39] depending on whether time-varying environment is taken into consideration.

Digital-domain SI cancellation methods cancel SI from quantified received signals after the analog-to-digital converter (ADC) [44]. A digital domain SI canceller first builds a baseband-equivalent model using the known transmit signal to capture everything between the DAC and ADC [42]. It then estimates linear and nonlinear components of SI based on the modeled channel to cancel the known transmit signal.

Compared to these SI cancellation approaches, FDMonitor does not know the transmitted signal, and thus we cannot simply subtract it to estimate the other signal. FDMonitor first works in the propagation domain with its bidirectional coupler to enhance isolation between transmitted and incident signals. However, the isolation is insufficient due to matching across a very wide band of SDR operation. FDMonitor applies a blind frequency-domain source separation algorithm in the digital domain for further signal separation.

2.3 Spectrum sensing

A shared platform's transmission could be monitored by repurposed spectrum sensing. Spectrum sensing [62] was proposed to sense primary users for opportunistic spectrum reuse, but it is, in essence, an approach to remotely detect transmission. Repurposed spectrum sensing can be categorized as (i) direct sensing, and (ii) cooperative sensing.

Direct sensing uses one node to locally sense a user's transmission [61]. It can be 1) transmitted signal prior-based sensing and 2) blind detection. The first type includes likelihood ratio test [62], cyclostationarity detection [49], waveform based sensing [57], and matched filtering [20]. These methods use priors including signal distributions, cyclostationarity, preamble and pilot pattern of the transmitted signals to be correlated with the received signal for signal presence detection. Blind detection, in contrast, does not require a prior [15]. It includes energy detection (ED) [13] or eigenvalue/covariance based detection [14]. ED measures the direct energy output whereas the latter uses the covariance matrix as an indicator of the received signal strength for presence classification.

Cooperative sensing utilizes measured signals sharing among collaborative radios to enhance the transmission

sensing performance [62]. The spatial distribution of multiple nodes effectively avoids hidden node problems and ameliorates degradation due to multipath fading and shadowing [32]. While cooperative sensing can be centralized, distributed and cluster-based [9], the fundamental sensing method is still direct sensing.

The above sensing techniques can be repurposed to monitor targeted transmissions of the shared SDR platform. However, it is unrealistic for us to require priors on the transmitted or incident signals; and blind methods will not be able to separate co-channel signals. In comparison, FDMonitor can precisely separate and identify both the transmitted signal and incident signal, even if they are on the same channel. It does use two measurements, thus like cooperative methods, it benefits from redundant measurements.

Bidirectional sensing. The preliminary work described in [59] reports on spectrum monitoring using a bidirectional coupler. That method assumes a known system model, and estimates the transmitted signal using the model inverse. However, system model calibration requires time-intensive manual effort. Furthermore, weather changes result in system variations which, if not recalibrated, reduce the separation performance. Experimentally, we also find the approach cannot sufficiently separate the transmitted and incident signals when they overlap in the frequency domain. In comparison to [59], FDMonitor provides several new benefits: 1) it is robust across signal type, carrier frequency, bandwidth and transmit power, 2) it enables mixing matrix estimation on the fly without system calibration, and 3) in addition to estimating the transmit signal, it *also* estimates the incident signal, which enables full-duplex monitoring.

3 SYSTEM DESIGN

We describe the design of FDMonitor, as shown in Figure 3, that can separate signals without a signal prior. The inputs to FDMonitor are the in-phase and quadrature (IQ) sampled signals at the two monitoring receiver channels, labeled R_0 and R_1 in Figure 2. Whenever the power in either channel is higher than the noise floor, we use the proposed algorithm to separate the signal into two sources. Given the power spectral density (PSD) limits defined by the platform operator, FDMonitor determines whether a violation occurred and reacts accordingly. In the following sections, describe the components of FDMonitor shown in Figure 3.

3.1 Problem Formulation

The overall goal of FDMonitor is to monitor the entire range of the platform, in our case 100–6000 MHz. The monitor samples from one band at a time, each with an RF bandwidth limited by the capability of the monitoring device (in our

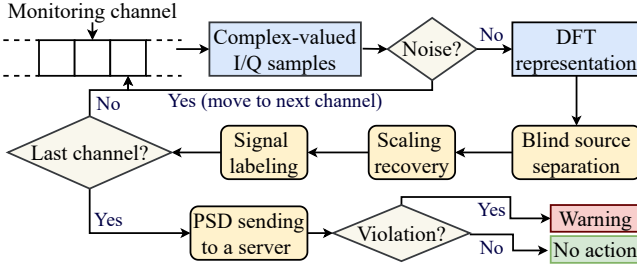


Figure 3: System components of FDMonitor

case, 27.65 MHz). We describe, without loss of generality, how FDMonitor operates on a single frequency band.

FDMonitor collects bidimensional samples $r_i(n)$ for sample $n = 0, 1, \dots, N - 1$ from ports $i = 0, 1$. Upon referring the source signals as $x_i(n)$ with $i = 0, 1$, we describe the bidimensional observations of the form:

$$\mathbf{r}(n) = \mathbf{A}\mathbf{x}(n) + \mathbf{v}(n), \quad \mathbf{v}(n) \sim \mathcal{CN}(\mathbf{0}, \sigma^2 \mathbf{I})$$

$$\mathbf{r}(n) = \begin{bmatrix} r_0(0) & \dots & r_0(N-1) \\ r_1(0) & \dots & r_1(N-1) \end{bmatrix} \in \mathbb{C}^{2 \times N} \quad (1)$$

$$\mathbf{x}(n) = \begin{bmatrix} x_0(0) & \dots & x_0(N-1) \\ x_1(0) & \dots & x_1(N-1) \end{bmatrix} \in \mathbb{C}^{2 \times N}.$$

Here $\mathbf{v}(n)$ is the zero-mean, uncorrelated additive Gaussian noise. We now present the assumptions based on (1) and discuss the major problem that needs to be addressed.

Assumption 1. *The observations $\mathbf{r}(n)$ are a noisy instantaneous linear mixture of source signals from $\mathbf{x}(n)$, and the system matrix $\mathbf{A} \in \mathbb{C}^{2 \times 2}$ is assumed to be unknown.*

Signal mixtures can be instantaneous or convolutive [24, 51]. We assume the former due to the fact that FDMonitor collects I/Q samples at the same time. We assume no prior knowledge of the system matrix \mathbf{A} so that calibration measurements are not required; and because weather and other changing conditions alter \mathbf{A} in practice. Instead, FDMonitor can adaptively estimate the linear model on the fly.

Assumption 2. *Source signals $x_0(n)$ and $x_1(n)$, for $n = 0, 1, \dots, N - 1$, are mutually independent and unknown. At most one of the source signals is Gaussian distributed.*

As the transmitted and incident signals, are from different sources: the SDR platform and outside world. One signal does not affect the other, leading to mutual independence. FDMonitor does not know what source signals are, as their properties are designed by platform users, and may even be proprietary and confidential.

Additionally, the noise power threshold in FDMonitor ensures that we do not operate source separation when both signals are purely noise. Given that digital signals are mostly non-Gaussian, assumption 2 holds.

Thus we design FDMonitor to solve the following problem:

Problem. *Given assumptions 1, 2 and the linear model in (1), the challenge is to estimate transmitted and incident signals from the received bidimensional measurements only, which is commonly referred as blind source separation (BSS) for instantaneous linear mixture.*

3.2 Frequency-domain ICA Modeling

We introduce a well-known BSS technique, independent component analysis (ICA), to address the problem. ICA approaches, according to [48], are identical to BSS solutions for instantaneous linear mixtures. They assume the same linear mixture framework as in (1) and require assumptions 1 and 2. ICA may be applied in either the time or frequency domain due to the linearity of Fourier transform. We adopt the frequency-domain ICA given the spectrum monitoring application of this work. In detail, complex-valued samples $r_i(n)$ for $i = 0, 1$ are first converted to frequency-domain components via Discrete Fourier Transform (DFT):

$$R_i(k) = \sum_{n=0}^{N-1} r_i(n) e^{-j \frac{2\pi}{N} kn}, \quad k = 0, 1, \dots, N - 1. \quad (2)$$

The linear model in (1) can then be rewritten in the frequency domain as:

$$\mathbf{R} = \mathbf{A}\mathbf{X} + \mathbf{V}, \quad \mathbf{V} \sim \mathcal{CN}(\mathbf{0}, N\sigma^2 \mathbf{I}), \quad (3)$$

where $\mathbf{R} = [R_0 \ R_1]^T \in \mathbb{C}^{2 \times N}$ are the DFT components of raw samples and \mathbf{V} in the frequency domain is still Gaussian distributed. The objective of frequency-domain ICA is to estimate the system matrix \mathbf{A} and source signals \mathbf{X} in (3) in each monitoring channel.

3.3 ICA for Source Separation

ICA methods include two steps for source separation: 1) data pre-processing and 2) contrast (cost) function optimization for estimating mixing matrix. Data pre-processing consists of data centering and whitening to produce zero-mean, uncorrelated components with unit variance [48]. For the second step, different contrast functions that quantify statistical independence have been proposed in the last two decades including cumulants, entropy, and mutual information [37]. With a selected contrast function, an ICA method can use Jacobi optimization or gradient-based schemes to iteratively estimate the system matrix [21].

The following ICA algorithms, as applicable to complex-valued signals, are considered in this paper: 1) Fast Independent Component Analysis (FastICA) [17]; 2) Joint Approximate Diagonalization of Eigen-matrices (JADE) [22]; and 3) Adaptable Complex Maximization of Nongaussianity (A-CMN) [50]. All three algorithms are widely used for various applications. However, FastICA and A-CMN require

some prior knowledge of the source distribution in order to optimally choose the contrast function [50]. Although this increases algorithm robustness, this knowledge is not generally available to SDR platform operators who want to accommodate as many wireless techniques as possible. Hence FDMonitor cannot limit the PHY to particular source distributions. JADE, which demands no such prior, is more adaptable to different source conditions and therefore has been used in FDMonitor. The JADE algorithm is shown in Algorithm 1. Note that the separated estimates after ICA have neither the same magnitude as that of raw samples nor correct labeling of “transmitted” vs. “incident”, due to two common ICA ambiguities we discuss in the next section.

Algorithm 1: The JADE algorithm

Data: DFT components of raw samples $\mathbf{R} \in \mathbb{C}^{2 \times N}$
Result: Source estimates $\tilde{\mathbf{X}}$ and the mixing matrix estimate $\tilde{\mathbf{A}}$

```

/* Data preprocessing */
 $\tilde{\mathbf{R}}(k) = \mathbf{R}(k) - \text{avg}(\mathbf{R}(k));$  /* centering */
 $\mathbf{E}, \mathbf{D} \leftarrow \text{EVD}(\text{Cov}\{\tilde{\mathbf{R}}(k)\});$ 
 $\tilde{\mathbf{D}} = \mathbf{D}^{-\frac{1}{2}} \mathbf{E}^H, \tilde{\mathbf{R}}(k) = \tilde{\mathbf{D}} \tilde{\mathbf{R}}(k);$  /* whitening */
/* Contrast function optimization */
for  $i, j, l, m = 0, 1$  do
|  $Q(\tilde{\mathbf{R}}) = \text{Cum}(\tilde{\mathbf{R}}_i, \tilde{\mathbf{R}}_j^H, \tilde{\mathbf{R}}_l, \tilde{\mathbf{R}}_m^H);$  /* kurtosis */
end
Compute  $\Phi = \{\lambda_i, M_i \mid i = 0, 1\}$  as the two largest
{eigenvalue, eigenmatrix} set of  $Q(\tilde{\mathbf{R}})$ ;
Compute a unitary matrix  $\tilde{\mathbf{U}}$  by jointly diagonalizing
 $\Phi$ ;
Compute  $\tilde{\mathbf{X}}(k) = \tilde{\mathbf{U}}^H \tilde{\mathbf{R}}(k)$ ;
Compute  $\tilde{\mathbf{A}} = \tilde{\mathbf{D}}^\# \tilde{\mathbf{U}}$ ; /*  $\tilde{\mathbf{D}}^\#$ : pseudoinverse */

```

3.4 Scaling and Permutation Alignment

ICA methods have two common problems: scaling ambiguities and permutation ambiguities. First, ICA solutions are scaled by an unknown constant. Second, the two signal estimates are arbitrarily assigned, thus it is not known which signal was “transmitted” which was “incident”. These ambiguities impose great challenges on violation detection as FDMonitor does not know which estimate to look at for violation detection, and which for environmental spectrum monitoring.

Assume that the two ICA estimates are each scaled by a multiplicative factor and may be permuted (i.e., swapped). These changes are modeled via the mixing matrix as:

$$\tilde{\mathbf{A}} \leftarrow \Lambda \tilde{\mathbf{A}} \mathbf{W}, \quad (4)$$

where Λ is a diagonal scaling matrix. $\hat{\mathbf{A}}$ is the ultimate mixing matrix to be obtained, and \mathbf{W} is either the 2×2 identity matrix, or if it is permuted, the 2×2 exchange matrix $\mathbf{J}_2 \triangleq \begin{bmatrix} 0 & 1 \\ 1 & 0 \end{bmatrix}$.

In the next sections, we first recover the scale via the estimated mixing matrix and address permutation ambiguity using correlation coefficients and power differences.

3.4.1 Scaling Alignment. We observe, from (4), that $\tilde{\mathbf{A}}$ having a norm larger than 1 essentially causes the scaling ambiguity challenge. To recover the scale, we first diagonalize the mixing matrix $\tilde{\mathbf{A}}$ to obtain a complex-valued diagonal matrix $\Delta(\tilde{\mathbf{A}})$:

$$\Delta(\tilde{\mathbf{A}}) = \text{Diag}\{\tilde{\mathbf{A}}\}. \quad (5)$$

The correct power level of the two estimates is then:

$$\hat{\mathbf{X}}(k) = \Delta(\tilde{\mathbf{A}}) \tilde{\mathbf{X}}(k), \quad k = 0, 1, \dots, N - 1. \quad (6)$$

3.4.2 Permutation Alignment. To simplify the problem, we first hypothesize the following: “transmitted” $\leftrightarrow \hat{X}_0(k)$, “incident” $\leftrightarrow \hat{X}_1(k)$. The permutation is incorrect if the hypothesis is false. As we know that $R_0(k)$ from port 0 detects more of the transmitted signal than port 1 does given by FDMonitor’s directionality, we first use the Pearson correlation coefficient [8] to test the hypothesis:

$$\text{corr}(|\hat{X}_i|, |\tilde{R}_j|) = \frac{\text{Cov}\{|\hat{X}_i|, |\tilde{R}_j|\}}{\sigma_{|\hat{X}_i|} \sigma_{|\tilde{R}_j|}}, \quad i, j = 0, 1, \quad (7)$$

where $|\cdot|$ denotes the magnitude of the complex value. $\text{Cov}\{\cdot\}$ is the covariance and σ is the standard deviation operator, calculated over all frequency samples k . We then are able to align the results based on the maximum of the four correlation values:

$$\hat{i}, \hat{j} = \arg \max_{i, j \in \{0, 1\}} \text{corr}(|\hat{X}_i|, |\tilde{R}_j|). \quad (8)$$

If indices $\hat{i} = \hat{j}$, regardless of the value, the hypothesis is correct. Otherwise, we multiply $\hat{\mathbf{X}}$ by the exchange matrix \mathbf{J}_2 to swap them back.

The above solution applies to all but source signals of similar power spectra shapes as the correlation coefficients, in this case, are closely high and hence unreliable. As a result, we propose to further align permutation via power maximum between $\tilde{\mathbf{R}}$ and $\hat{\mathbf{X}}$ if the correlation coefficients fall out of the 95% confidence interval. Specifically, If \tilde{R}_0 has more power than \tilde{R}_1 , \hat{X}_0 should correspondingly have higher magnitude than \hat{X}_1 . Therefore the \tilde{R}_j and \hat{X}_i with higher power are matched.

3.4.3 Mixing Matrix Adjustment. Certain adjustments of the estimated mixing matrix $\hat{\mathbf{A}}$ are needed to properly account for the changes we made for scaling and permutation alignment in Section 3.4.1 and 3.4.2. The final estimated

mixing matrix is:

$$\hat{\mathbf{A}} = (\Delta(\tilde{\mathbf{A}}))^{-1} \tilde{\mathbf{A}} \mathbf{W} \quad (9)$$

where $(\Delta(\tilde{\mathbf{A}}))^{-1}$ is the scaling recovery matrix and \mathbf{W} is the permutation recovery matrix: if permutation occurs, $\mathbf{W} = \mathbf{J}_2$, otherwise it is the 2x2 identity matrix.

3.5 Performance evaluation

We propose a new evaluation metric here to quantitatively evaluate the ability of FDMonitor to separate the sources. In particular, we do not want the algorithm to “blame” the user for the incident signal, nor do we want to corrupt the incident signal estimate with the user’s transmitted signal. The principle is that the power spectral density (PSD) of \hat{X}_0 should be high, and much lower in \hat{X}_1 , over the frequencies containing the transmitted signal. Similarly the PSD of \hat{X}_1 should be high, and much lower in the \hat{X}_0 , over the frequencies where there is an incident signal.

To define the metric, we define a frequency band (set) \mathcal{B}_{Tx} to contain frequency indices in which the node is transmitting; and set \mathcal{B}_{In} to contain frequency indices in which there is incident signal. We compute the average PSDs of these signals in estimated signals $\hat{X}_i(k)$, for $i = 0, 1$, as:

$$\begin{aligned} P_i[Tx] &= \frac{1}{|\mathcal{B}_{Tx}|} \sum_{k \in \mathcal{B}_{Tx}} |\hat{X}_i(k)|^2 \\ P_i[In] &= \frac{1}{|\mathcal{B}_{In}|} \sum_{k \in \mathcal{B}_{In}} |\hat{X}_i(k)|^2. \end{aligned} \quad (10)$$

We then define the *transmit in port 0 to transmit in port 1* ratio (TTR) and the *incident in port 1 to incident in port 0* ratio (IIR) as:

$$\text{TTR}_{0 \rightarrow 1} = \frac{P_0[Tx]}{P_1[Tx]}, \quad \text{IIR}_{1 \rightarrow 0} = \frac{P_1[In]}{P_0[In]}. \quad (11)$$

Similar to signal to interference ratio (SIR), our TTR and IIR values measure a power ratio. However, TTR and IIR do not require exact knowledge of the true transmitted and incident signals $X_0(k)$ and $X_1(k)$ for all k , which is unavailable, even during experiments. Our metrics, TTR and IIR, focus specifically on the isolation performance of FDMonitor rather than the quality of $\hat{X}_0(k)$ and $\hat{X}_1(k)$ individually.

4 IMPLEMENTATION

In this section, we present the implementation of FDMonitor on a large-scale wireless testbed. We first discuss the monitoring hardware, and specifications of their use in the experiments. Finally, the signal separation algorithm is given in Algorithm 2.

4.1 Monitoring Hardware

We use the following hardware in our experiments: (1) an SDR transmitter and incidental source each controlled via USB by an Intel NUC computer, (2) our custom bidirectional coupler connected between the TX port and antenna, (3) the monitor node connected to the two output ports of the bidirectional coupler, and (4) a wide-band antenna [5].

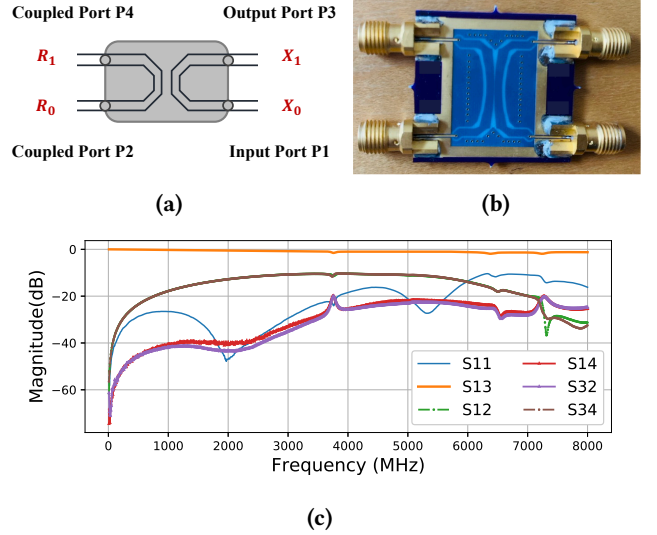


Figure 4: Bidirectional coupler (a) port diagram; (b) realization on PCB; (c) measured S-parameters. While extremely wideband and low loss, the isolation between coupled ports can be as low as 10 dB.

We use a NUC, a small-form-factor PC with an Intel Core I7-8650 processor and 32 GB of DDR4 RAM, running Ubuntu 18.04 LTS. Our monitor and node SDR are both NI USRP B210s, which are able to transmit and receive in the spectrum range from 70–6000 MHz [29], with a sample rate up to 61 MSps. The antenna used is a TAOGLAS wide-band 4G LTE I-Bar, effective across a 698–6000 MHz band [58].

A critical component of the RF monitoring system, a bidirectional coupler, is designed and built as shown in Figure 4a and 4b. It has four ports: P1 and P3 are input and output ports representing direct transmission whereas P2 and P4 are coupled ports that can capture mixed signals at different scales. To show the directionality of the coupler when it is isolated, we measure its S-parameters across the 100–6000 MHz frequency range, as shown in Figure 4c. S_{11} shows low return loss, below -10 dB across the band. S_{13} is close to 0 for the wide spectrum, indicating little power loss of the direct transmit signal from P1 to P3. In addition, S_{12} and S_{14} show that P2 and P4 receive a copy of the transmitted signal that is at least 10 dB and 20 dB down from the transmitted

signal power, respectively. Likewise, S_{32} and S_{34} show that the samples collected in P4 and P2 are at least 20 dB and 10 dB down from the incident signal power.

4.2 Monitoring Software

To monitor the entire 100–6000 MHz range, FDMonitor divides the spectrum into multiple smaller frequency channels. Issues with the NI B210 sometimes results in invalid samples when run at its maximum sampling rate, thus we use a sampling rate of 27.65 MSps, a factor of 0.9 of its maximum two-channel sampling rate. To cover the entire monitoring spectrum, 214 monitoring channels must be iterated through. For the results here, in each channel, $N = 2 \times 10^4$ complex-valued samples are collected by FDMonitor for source separation and mixing matrix estimation.

The FDMonitor procedure is detailed in Algorithm 2. Note that PSD limits may be user-dependent, and we assume that they are known to the algorithm. Our implementation notifies the user and staff of the problem. Future implementations could be set to automatically shut off the transmitter.

5 RESULTS

In this section, experimental results of FDMonitor are presented using the setup shown in Figure 2.

Baseline method. We use our preliminary work in [59] as a baseline to compare to FDMonitor. The baseline, *System Matrix Calibration (SMC)*, works as follows. SMC first calibrates the system matrix, at each frequency bin, by placing the system in a RF isolation area. In detail, a known signal is first transmitted by the experimental SDR and is received by the monitoring system at two ports. A spectrum analyzer captures the actual transmitted signal X_0 . As the incident signal is zero, half of the mixing matrix can be estimated by comparing the measurements R and X_0 . Similarly, by setting $X_0 = 0$ and transmitting a signal from an incident source (as measured by a spectrum analyzer), the other half of the mixing matrix is obtained. The calibrated linear model is then inverted and, during operation, is used to separate the transmitted and incident signals.

5.1 Source Separation of FDMonitor

Our first experiments are designed to answer the following critical question: **Can FDMonitor separate and identify signals of different modulations, center frequencies and bandwidths, and relative power levels?** We conduct multiple controlled experiments, in which we set the transmit signal, and create an environmental signal that impinges on the platform antenna, to answer this question.

5.1.1 Signal Type. First, we run an experiment in which an OFDM signal is transmitted at 3670 MHz and a BPSK signal is incident at 3659 MHz. Both have a bandwidth of

Algorithm 2: Algorithmic Operation of FDMonitor

Result: TX/incident signals, alert notification
Initialize user PSD limits vs. frequency;
Initialize the list of channel center frequencies f_{list} ;
while True do
 for f **in** f_{list} **do**
 Sample $r_i(n)$ for $i = 0, 1$ & $n = 0 \dots N - 1$;
 $R_i(k) \leftarrow FFT\{r_i(n), i = 0, 1\}$; /* Sec.3.2 */
 $\tilde{X}(k), \tilde{A} \leftarrow JADE\{R(k)\}$; /* Sec.3.3 */
 $\hat{X} \leftarrow \Delta(\tilde{A})\tilde{X}(k)$;
 $\hat{A} \leftarrow (\Delta(\tilde{A}))^{-1} \tilde{A}$; /* Scaling */
 if $corr(|\hat{X}_i|, |\tilde{R}_m|) > 0.95 \forall i, m = 0, 1$ **then**
 $i \leftarrow \arg \max_i (|\hat{X}_i|)$, $i = 0, 1$
 $m \leftarrow \arg \max_m (|\tilde{R}_m|)$, $m = 0, 1$;
 else
 $i, m \leftarrow \arg \max_{i,m} cor(|\hat{X}_i|, |\tilde{R}_m|)$;
 end
 if $i \neq m$ **then**
 $\hat{X}(k) = J_2 \cdot \hat{X}(k)$;
 $\hat{A} = J_2 \cdot \hat{A}$; /* Permutation */
 end
 end
Concatenate $\hat{X}(k)$ for all frequency channels f ;
Compute $PSD = 10 \log_{10} |\hat{X}_0(k)|^2$;
if $PSD > user\ PSD\ limits$ **then**
 Notify & send PSD graph to user & staff;
end
end

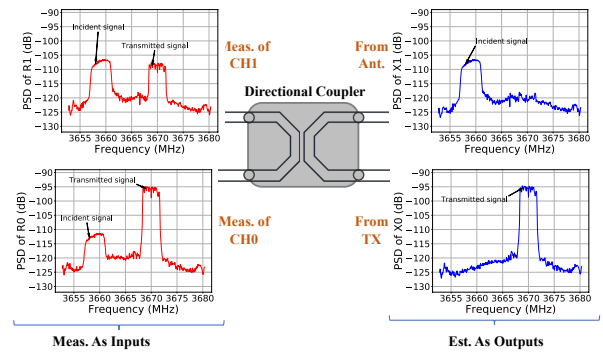


Figure 5: Different types of signals: FDMonitor almost completely separates an OFDM transmitted signal from BPSK incident signal. Improved TTR (13.12→27.78 dB) and IIR (6.33→17.36 dB).

4 MHz. The results in Figure 5 plot the PSD of R_0 and R_1

Types		Reference		SMC		FDMonitor	
transmitted signals	incident signals	TTR (dB)	IIR (dB)	TTR (dB)	IIR (dB)	TTR (dB)	IIR (dB)
CW	OFDM	13.30	7.21	30.92	3.54	30.95	19.60
OFDM	CW	12.56	6.91	22.61	7.39	29.60	18.14
CW	BPSK	13.38	6.02	30.24	4.48	30.26	16.33
BPSK	CW	12.55	6.40	20.06	8.32	28.06	18.65
OFDM	BPSK	13.12	6.33	22.64	5.60	29.68	16.36
BPSK	OFDM	13.17	7.76	20.48	3.85	28.48	19.48

Table 1: TTR & IIR for transmitted/incident signals of three types. SMC increases signal isolation in CW scenarios only. FDMonitor provides more isolation and is effective across all signal types.

on the left, showing them at different power levels due to directionality of the coupler. The right plots of Figure 5 show that only the correctly scaled transmitted signal remains in FDMonitor’s output, \hat{X}_0 . Likewise, the transmitted signal has been fully eliminated from the incident signal estimate \hat{X}_1 .

We further compare FDMonitor to SMC with typical digital signal types, CW, BPSK, and OFDM, using TTR and IIR. The results in Table 1 show that both methods increase isolation of the transmitted signal. However, we observe two disadvantages of SMC. First, it cannot improve TTR as FDMonitor in CW transmission scenarios. Consider the first case with CW and OFDM: the reference TTR is 13.3 dB. SMC and FDMonitor enhance the isolation by similar amounts, 16.6 and 16.6 dB, respectively. However, large TTR differences in modulated transmitted signals expose the inability of SMC to remove the transmitted signal from X_1 . When the transmitted signal is either OFDM or BPSK, the TTR increase via SMC is only 10 dB or 7 dB compared to 17 or 15 dB using FDMonitor. Secondly, SMC shows only a small IIR increase when the incident signal is CW, but inadvertently reduces the isolation for other signals. In the best case (row 4), SMC only increases IIR by 1.9 dB. In comparison, large IIR increases obtained using FDMonitor for all signal types indicate accurate and robust estimation of source signals.

5.1.2 Carrier and Center Frequency. Can FDMonitor separate signals that overlap in the frequency domain? We conduct an experiment with two overlapping OFDM signals that overlap: an incident signal (5758–5762 MHz) and a transmitted signal (5756–5760 MHz) that overlap between 5758–5760 MHz. The separation results in Figure 6 show complete removal of the incident signal from X_0 , and complete removal of the transmit signal from X_1 .

To check the consistency of the separation performance across frequency at the receiver, experiments are conducted in the 2.4 GHz and 5.8 GHz ISM and 3.6 GHz CBRS bands, while transmitting non-overlapping CW signals. In Figure 7,

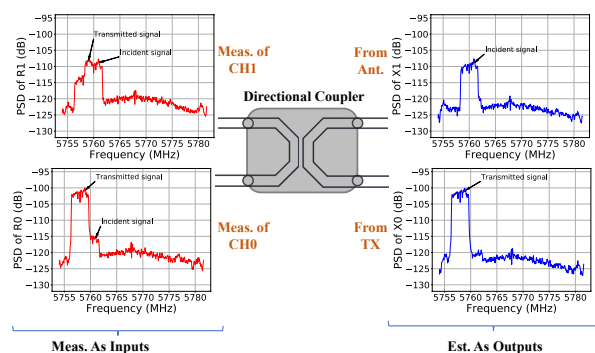


Figure 6: Frequency overlap: FDMonitor separates overlapping transmitted and incident OFDM signals. Only the incident signal remains in X_1 , and only the transmitted in X_0 .

we show that both methods increase the TTR across frequency, which means there is little impact of center frequency on either algorithm. Nevertheless, the large difference shown in IIR indicates poor incident signal separation of SMC and robust estimation via FDMonitor.

5.1.3 Signal Bandwidth. The transmitted and incident signal properties are unknown to FDMonitor, and might both occupy large bandwidths. We next run tests to explore how the performance of FDMonitor is affected by signal bandwidth.

In this experiment, we consider two OFDM signals: the transmitted signal is 10 MHz wide, centered at 2454 MHz, while the incident signal is at 2442 MHz with 4 MHz bandwidth. Figure 8 shows the incident signal in R_0 is removed from \hat{X}_0 . Equivalently, the transmitted signal has been mostly eliminated in \hat{X}_1 from R_1 . Notably, 4 dB energy of the transmit signal on the edges remains in the \hat{X}_0 . In addition, the spike at 2458 MHz has been confirmed (via separate investigation) as an environmental interference signal. This observation

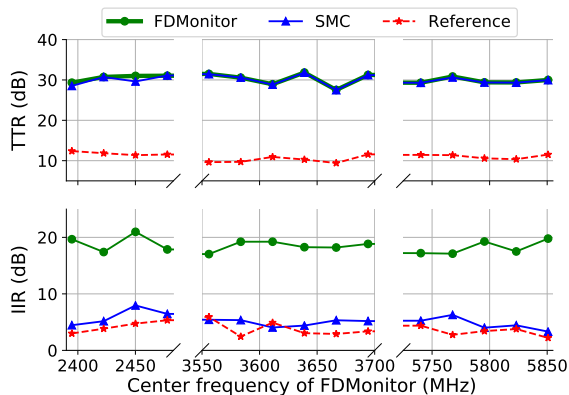


Figure 7: TTR and IIR vs. frequency. Both methods can estimate the incident signal, but FDMonitor results in superior IIR.

indicates that FDMonitor can perform source separation in the presence of multiple incident signals.

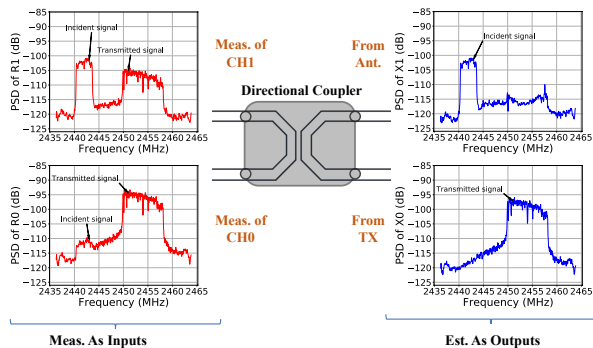


Figure 8: Different bandwidths: Signals of bandwidths 10 MHz & 4 MHz are separated.

Figure 9 shows how TTR and IIR change as the transmit signal bandwidth varies from 1 to 10 MHz (10 MHz is the maximum bandwidth a user can reserve for one experiment on the platform under test). FDMonitor is stable across bandwidth, but SMC demonstrates decreasing TTR with higher bandwidth. Additionally, the IIR for SMC is stable but much lower than the IIR reference, whereas FDMonitor produces higher IIR. Reduced IIR means there is a higher level of incident signal in \hat{X}_0 than in R_0 , a negative result.

5.1.4 **Signal Power.** Power difference as described in Section 3.4, can be used for solving permutation ambiguity. However, close power level may further confuse FDMonitor. Therefore, we present FDMonitor’s separation performance as a function of signal power.

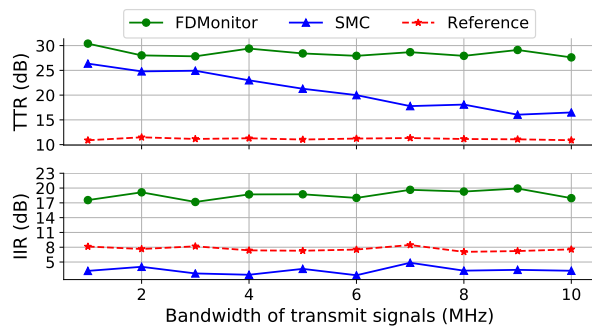


Figure 9: TTR and IIR variation vs. transmitted signal bandwidth. SMC degrades as bandwidth increases, whereas FDMonitor is consistent across bandwidth.

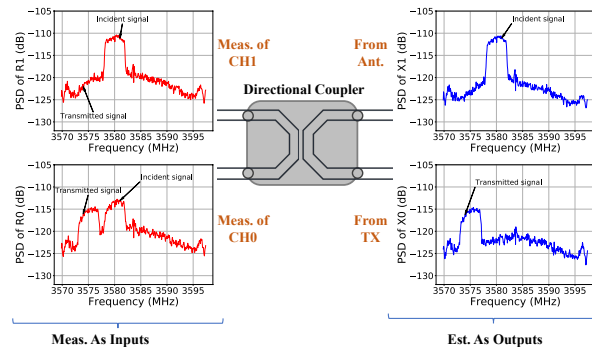


Figure 10: Similar Powers: FDMonitor separates BPSK signals despite similar power levels, -115 and -113 dB, increasing TTR ($5.9 \rightarrow 9.6$ dB) and IIR ($2.1 \rightarrow 10.6$ dB).

Figure 10 shows the separation of two BPSK signals with close power levels, with the transmitted signal centered at 3575 MHz. As the transmitted signal gain is low, it is nearly invisible in the PSD of $R_1(k)$. Despite the low-power transmit signal, the results show that FDMonitor accurately estimates and identifies each signal.

Finally, we vary transmitter gain as shown in Figure 11. The TTR and IIR for the reference method are approximately 10 and 5 dB. After running the two source separation algorithms, we make the following observations: (1) TTR for both methods increases while gain increases from 10 to 55 dB. (2) FDMonitor obtains higher TTR than SMC at each gain setting. (3) SMC provides IIR results around 2–3 dB lower than the reference, while FDMonitor increases IIR by 10–13 dB.

5.2 Algorithm Efficiency

We compare the two systems’ efficiency via latency. Latency in our work refers to elapsed time for frequency tuning, data collection and further analysis. Wideband monitoring

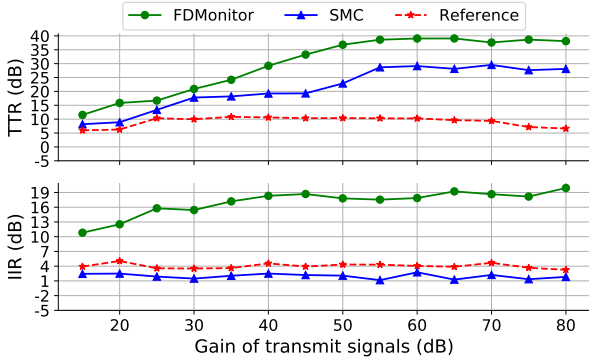


Figure 11: TTR and IIR vs. transmitter gain: Both improve with increasing gain in FDMonitor.

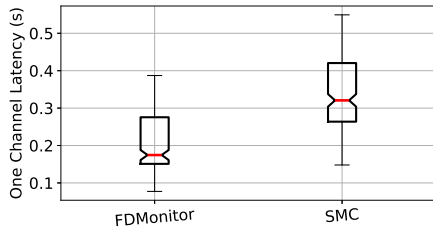


Figure 12: Latency of FDMonitor and SMC.

of RF utilization involves two main components, frequency sweeping and source separation. The former tunes the center frequency of the receiver while the latter provides transmitted signal estimation in each 27.65 MHz sub-band. To assess the methods in terms of efficiency, latency is measured in each monitoring channel. Figure 12 shows that, for monitoring one channel, the median latency of FDMonitor is 0.17 s whereas SMC requires 0.32 s. Given the median latency, the total time spent by FDMonitor to sweep the 100-6000 MHz spectrum is 36.4 s, half the latency of SMC.

5.3 Mixing Matrix Evaluation

We further evaluate the system performance via the mixing matrix $\hat{A} \in \mathbb{C}^{2 \times 2}$, which describes the linear system model for source separation, which is estimated on the fly. We collect mixing matrix and precipitation data for 29 days while continuously transmitting CW signals from both sources.

Figure 13 shows the mixing matrix magnitude vs. precipitation and monitoring hours. First, we observe that the matrix magnitude is relatively stable across 29 days. Both a_{11} and a_{22} are centered at 0.01 dB with 0.002 dB standard deviation. Noisier a_{21} and a_{12} are around -19.29 and -7.10 dB respectively with 0.094 and 0.075 dB standard deviation. In addition, we notice that the matrix varies with rainfall. At

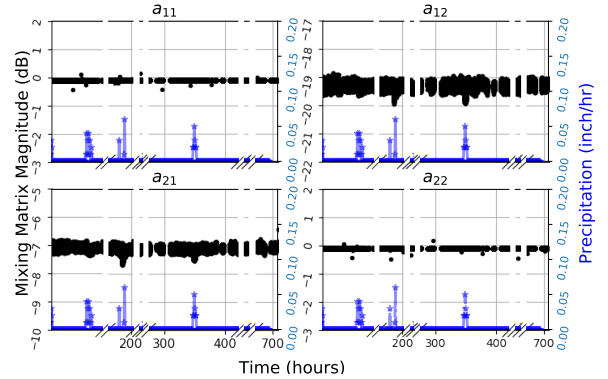


Figure 13: Mixing matrix magnitude over 105 hrs, with rain data. The magnitudes of matrix values are stable, but a_{21} & a_{21} change while surfaces are wet due to rain.

around 72, 187 and 348 hours, the magnitude of a_{21} and a_{21} decreases when rain starts and later goes back to the same pre-rain level. This can be explained by the change in the radio propagation environment for wet vs. dry surfaces [35]. This is another reason why the baseline SMC method, which learns the system matrix only once during calibration, is not robust compared to FDMonitor.

5.4 System-wide 7 Month Deployment

FDMonitor has been continuously monitoring 19 SDR platforms on the testbed, all deployed at different geographical locations, for more than 7 months. We evaluate its system-wide performance by investigating each violation alarm it generates during the period, and considering the alarm accuracy. A violation alarm notifies the user via email of detected signals being transmitted outside the declared spectrum. It can be a true detection of RF emission misbehavior, or a false alarm if the alert did not correspond to a user violating spectrum rules. We store measurements from each alert, and request information from the user about their setup in order to determine the ground truth about spectrum use.

The true violations so far, we classify into 5 types:

- (1) No declaration of any spectrum before using it,
- (2) High gain setting induces harmonics,
- (3) Adjacent band spillover w/ wideband TX signals,
- (4) 15 MHz intermodulation distortion, and
- (5) FDMonitor testing after installation.

Table 2 shows our analysis of the 662 total alerts. In sum, we observe only 20 false alarms, among which 13 alerts occurred because the user-declared frequency was, due to a software error, not recorded to the FDMonitor user PSD limits database. The other 7 false discovery emails were triggered by incorrectly resolved permutation ambiguities. Even

Type	False positives: 20 emails			True positives: 642 emails			
Rate	False discovery rate (FDR): 3.02%			Positive predictive value (PPV): 96.98%			
Cause	Bug: Spectrum declaration lost	Permutation ambiguity	No spectrum declaration	High gain induced harmonics	Signal spillover	Intermod. distortions	System testing
Rate	65%	35%	67.29%	18.54%	0.16%	10.28%	3.74%

Table 2: FDMonitor alert accuracy during continuous monitoring of 19 shared SDR platforms for > 7 months.

so, the 96.98% positive predictive value (PPV) represents high accuracy and robustness of FDMonitor across a large variety of real users, their signals, and the varying weather seen by the platform.

5.5 Adversarial Behavior

If FDMonitor sequentially monitors frequency channels to cover the entire 100-6000 MHz band, adversarial users can potentially transmit in violation while hopping between channels to avoid detection. To model adversarial behaviors, we use the following notation: 1) ΔT is the time duration to monitor one channel, 2) N_C is the total number of channels (in our case, 214), and 3) T denotes the cycle number, where each cycle corresponds to monitoring all N_C channels.

Attack model We propose the following attack model: 1) an attacker can use any channel at any given time, 2) in each time slot ΔT , an attacker chooses 1 of the N_C channels to transmit, 3) an attacker does not know which channel is being monitored.

Countermeasure To address this attack model, FDMonitor can no longer use a predictable monitoring scheme. Instead, we propose a countermeasure that randomizes the order: 1) in each monitoring cycle, FDMonitor generates a random permuted channel sequence of length N_C for spectrum monitoring, 3) all channels are measured by FDMonitor in each cycle. *The probability of first detecting an attacker at cycle T using the proposed countermeasure is:*

$$P_D(T) = \left(\frac{N_C - 1}{N_C}\right)^{N_C(T-1)} \left(1 - \left(\frac{N_C - 1}{N_C}\right)^{N_C}\right). \quad (12)$$

$P_D(1)$ asymptotically converges to $1 - \frac{1}{e}$ or 63% as $N_C \rightarrow \infty$. The average number of cycles for attacker detection is $1/P_D(1)$, which for high N_C is 1.58 cycles. The proof is omitted due to space constraints. For validation, we show in Figure 14 results of a simulation run 10^4 times at each N_C .

We describe one type of adversarial behavior above. However, other adversarial behaviors are also possible. For instance, an adversary can use a particular channel for a duration longer than ΔT . In this situation, the probability of detecting the adversary, $P_D(T)$ will actually be higher. In a different pathological scenario, an adversarial testbed user

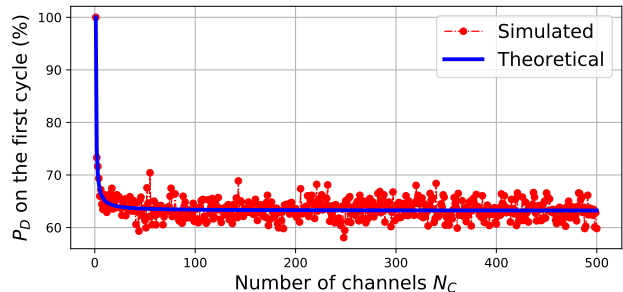


Figure 14: Prob. of detecting violation in the first cycle. In FDMonitor, $N_C = 214$, and thus $P_D(1) = 65.18\%$.

can have a colluder externally transmit the same disallowed signal that the user transmits, in a time-synchronized manner. If the external incoming signal is at sufficiently high power, FDMonitor can miss detecting the user signal. We will investigate such pathological adversarial cases in our future work.

6 DISCUSSION

We describe some limitations of FDMonitor and discuss the implications for future research.

Non-Gaussian constraint One constraint of FDMonitor is Assumption 2 that at most one of the sources is Gaussian. One possible solution is that, if both signals are found to be Gaussian, FDMonitor could use a recently estimated system matrix \hat{A} for separation instead of estimating it on the fly.

Generalization to MIMO platforms Generally, one FDMonitor is needed for each transmit antenna, since it currently relies on a bidirectional coupler to separate the transmit and incident signal to that antenna. This could be a scaling problem for MIMO platforms. However, future work could use a $(N + 1)$ -directional coupler for monitoring N -antenna MIMO platforms assuming that the incident signal appears in different linear combinations on all antennas. By doing so, $N + 1$ rather than $2N$ measurements would be needed for MIMO ICA separation.

7 CONCLUSION

This paper proposes, implements, and reports on FDMonitor, a robust and continuous full-duplex monitoring system for effective supervision of a SDR platform's transmissions and environmental use of spectrum. FDMonitor uses a novel frequency-domain source separation algorithm to distinguish signals of the SDR platform from those incident on the antenna. Critically, our approach does not require extensive calibration, which would be very challenging to implement at the rate at which calibration becomes obsolete. Its performance is extensively validated with four different types of RF signal experiments, across communication signal types, carrier frequency, bandwidth and transmit power. We evaluated more than 7 months of live system performance, which generates a low 3.02% FDR, with 20 false alerts.

8 ACKNOWLEDGMENT

This research is supported in part by the US National Science Foundation Grants 1564287 and CNS-1827940, and the PAWR Industry Consortium.

REFERENCES

- [1] Open-access research testbed for next-generation wireless networks (ORBIT), 2005. <https://www.orbit-lab.org/>.
- [2] Bristol Is Open, 2013. <https://www.bristol.gov.uk/policies-plans-strategies/bristol-is-open>.
- [3] The ADRENALINE testbed, 2017. <http://networks.cttc.es/ons/adrenaline/>.
- [4] 5G PPP platforms cartography, 2018. <https://5g-ppp.eu/5g-ppp-platforms-cartography/>.
- [5] Intel® NUC kit NUC7i7DNHE, 2018. <https://ark.intel.com/content/www/us/en/ark/products/130393/intel-nuc-kit-nuc7i7dnhe.html>.
- [6] Platforms for advanced wireless research (PAWR) program, 2018. <https://advancedwireless.org/>.
- [7] The European 5G annual journal. Technical report, Full 5G – Supporting the European 5G Initiative, 2021.
- [8] Haldun Akoglu. User's guide to correlation coefficients. *Turkish Journal of Emergency Medicine*, 18(3):91–93, 2018.
- [9] Ian F. Akyildiz, Brandon F. Lo, and Ravikumar Balakrishnan. Cooperative spectrum sensing in cognitive radio networks: A survey. *Physical Communication*, 4(1):40 – 62, 2011.
- [10] Ian F. Akyildiz, Shuai Nie, Shih-Chun Lin, and Manoj Chandrasekaran. 5G roadmap: 10 key enabling technologies. *Computer Networks*, 106:17–48, 2016.
- [11] Muhammad Amjad, Fayaz Akhtar, Mubashir Husain Rehmani, Martin Reisslein, and Tariq Umer. Full-duplex communication in cognitive radio networks: A survey. *IEEE Communications Surveys Tutorials*, 19(4):2158–2191, 2017.
- [12] Ehsan Aryafar, Mohammad Amir Khojastepour, Karthikeyan Sundaresan, Sampath Rangarajan, and Mung Chiang. MIDU: Enabling MIMO full duplex. In *Proceedings of the 18th Annual International Conference on Mobile Computing and Networking*, Mobicom '12, page 257–268, 2012.
- [13] Saman Atapattu, Chintha Tellambura, and Hai Jiang. Energy detection based cooperative spectrum sensing in cognitive radio networks. *IEEE Transactions on Wireless Communications*, 10(4):1232–1241, 2011.
- [14] Farooq Awain, Esam Abdel-Raheem, and Kemal Tepe. Blind spectrum sensing approaches for interweaved cognitive radio system: A tutorial and short course. *IEEE Communications Surveys Tutorials*, 21(1):238–259, 2019.
- [15] Erik Axell, Geert Leus, Erik G. Larsson, and H. Vincent Poor. Spectrum sensing for cognitive radio : State-of-the-art and recent advances. *IEEE Signal Processing Magazine*, 29(3):101–116, 2012.
- [16] Dinesh Bharadia, Emily McMillin, and Sachin Katti. Full duplex radios. *SIGCOMM Comput. Commun. Rev.*, 43(4):375–386, aug 2013.
- [17] Ella Bingham and Aapo Hyvärinen. A fast fixed-point algorithm for independent component analysis of complex valued signals. *International Journal of Neural Systems*, 10:1–8, 03 2000.
- [18] Joe Breen, Andrew Buffmire, Jonathon Duerig, Kevin Dutt, Eric Eide, Mike Hibler, David Johnson, Sneha Kumar Kasera, Earl Lewis, Dustin Maas, Alex Orange, Neal Patwari, Daniel Reading, Robert Ricci, David Schurig, Leigh B. Stoller, Jacobus Van der Merwe, Kirk Webb, and Gary Wong. POWDER: Platform for open wireless data-driven experimental research. In *Proceedings of the 14th International Workshop on Wireless Network Testbeds, Experimental Evaluation and Characterization (WiNTECH)*, September 2020.
- [19] US FCC Enforcement Bureau. Enforcement overview, April 2020. https://www.fcc.gov/sites/default/files/public_enforcement_overview.pdf.
- [20] Danijela Cabric, Artem Tkachenko, and Robert W. Brodersen. Spectrum sensing measurements of pilot, energy, and collaborative detection. In *2006 IEEE Military Communications Conference*, pages 1–7, 2006.
- [21] Jean-François Cardoso. High-order contrasts for independent component analysis. *Neural computation*, 11(1):157–192, 1999.
- [22] Jean François Cardoso and Antoine Souloumiac. Blind beamforming for non-gaussian signals. *IEEE Proceedings F - Radar and Signal Processing*, 140(6):362–370, 1993.
- [23] John M. Chapin. Spectrum innovation initiative: National radio dynamic zones (SII-NRDZ) program solicitation, 2022. <https://www.nsf.gov/pubs/2022/nsf22579/nsf22579.htm>.
- [24] Seungjin Choi, Andrzej Cichocki, Hyung-Min Park, and Soo-Young Lee. Blind source separation and independent component analysis: A review. *Neural Information Processing-Letters and Reviews*, 6(1):1–57, 2005.
- [25] Federal Communications Commission. OET experimental licensing system. <https://apps.fcc.gov/oetcf/els/index.cfm>.
- [26] Federal Communications Commission. Report and order and second further notice of proposed rulemaking, April 2015. GN Docket No. 12-354, FCC 15-47, https://www.fcc.gov/sites/default/files/public_enforcement_overview.pdf.
- [27] Xavier Pérez Costa, Joerg Swetina, Tao Guo, Rajesh Mahindra, and Sampath Rangarajan. Radio access network virtualization for future mobile carrier networks. *IEEE Communications Magazine*, 51:27–35, 2013.
- [28] Melissa Duarte, Chris Dick, and Ashutosh Sabharwal. Experiment-driven characterization of full-duplex wireless systems. *IEEE Transactions on Wireless Communications*, 11(12):4296–4307, 2012.
- [29] Matt Ettus and Martin Braun. The universal software radio peripheral (USRP) family of low-cost sdrs. In *Opportunistic Spectrum Sharing and White Space Access*, pages 3–23, 2015.
- [30] Wireless Innovation Forum. Spectrum access system (SAS) - citizens broadband radio service device (CBSD) interface technical specification. 2020.
- [31] Xenofon Foukas, Georgios Patounas, Ahmed Elmokashfi, and Mahesh K. Marina. Network slicing in 5G: Survey and challenges. *IEEE Communications Magazine*, 55(5):94–100, 2017.
- [32] Amir Ghasemi and Elvino S. Sousa. Spectrum sensing in cognitive radio networks: requirements, challenges and design trade-offs. *IEEE*

Communications Magazine, 46(4):32–39, 2008.

- [33] Mohammad Asif Habibi, Meysam Nasimi, Bin Han, and Hans D. Schotten. A comprehensive survey of RAN architectures toward 5G mobile communication system. *IEEE Access*, 7:70371–70421, 2019.
- [34] Paul Harris, Wael Boukley Hasan, Henry Brice, Benny Chitambira, Mark Beach, Evangelos Mellios, Andrew Nix, Simon Armour, and Angela Doufexi. An overview of massive MIMO research at the university of bristol. In *Radio Propagation and Technologies for 5G (2016)*, pages 1–5, 2016.
- [35] Peter Hillyard, Anh Luong, and Neal Patwari. Highly reliable signal strength-based boundary crossing localization in outdoor time-varying environments. In *2016 15th ACM/IEEE International Conference on Information Processing in Sensor Networks (IPSN)*, pages 1–12, 2016.
- [36] Feng Hu, Bing Chen, and Kun Zhu. Full spectrum sharing in cognitive radio networks toward 5G: A survey. *IEEE Access*, 6:15754–15776, 2018.
- [37] Aapo Hyvärinen and Erkki Oja. Independent component analysis: Algorithms and applications. *Neural networks : the official journal of the International Neural Network Society*, 13:411–30, 06 2000.
- [38] Intel. vRAN: The next step in network transformation. *White Paper*, 2017.
- [39] Mayank Jain, Jung Il Choi, Taemin Kim, Dinesh Bharadia, Siddharth Seth, Kannan Srinivasan, Philip Levis, Sachin Katti, and Prasun Sinha. Practical, real-time, full duplex wireless. In *Proceedings of the 17th Annual International Conference on Mobile Computing and Networking, MobiCom '11*, page 301–312, 2011.
- [40] Miao Jiang, Yiqing Li, Qi Zhang, Guangchi Zhang, and Jiayin Qin. Decentralized blockchain-based dynamic spectrum acquisition for wireless downlink communications. *IEEE Transactions on Signal Processing*, 69:986–997, 2021.
- [41] Edwin Jonathan Kitindi, Shu Fu, Yunjian Jia, Asif Kabir, and Ying Wang. Wireless network virtualization with SDN and C-RAN for 5G networks: Requirements, opportunities, and challenges. *IEEE Access*, 5:19099–19115, 2017.
- [42] Kenneth E. Kolodziej, Bradley T. Perry, and Jeffrey S. Herd. In-band full-duplex technology: Techniques and systems survey. *IEEE Transactions on Microwave Theory and Techniques*, 67(7):3025–3041, 2019.
- [43] Chengchao Liang and F. Richard Yu. Wireless network virtualization: A survey, some research issues and challenges. *IEEE Communications Surveys Tutorials*, 17(1):358–380, 2015.
- [44] Gang Liu, F. Richard Yu, Hong Ji, Victor C. M. Leung, and Xi Li. In-band full-duplex relaying: A survey, research issues and challenges. *IEEE Communications Surveys Tutorials*, 17(2):500–524, 2015.
- [45] Vuk Marojevic, Ismail Guvenc, Rudra Dutta, Mihail L. Sichitiu, and Brian A. Floyd. Advanced wireless for unmanned aerial systems: 5G standardization, research challenges, and AERPAAW architecture. *IEEE Vehicular Technology Magazine*, 15(2):22–30, 2020.
- [46] Rashid Mijumbi, Joan Serrat, Juan-Luis Gorricho, Niels Bouten, Filip De Turck, and Raouf Boutaba. Network function virtualization: State-of-the-art and research challenges. *IEEE Communications Surveys Tutorials*, 18(1):236–262, 2016.
- [47] Raul Muñoz, Laia Nadal, Ramon Casellas, Michela Svaluto Moreolo, Ricard Vilalta, Josep Maria Fàbrega, Ricardo Martínez, Arturo Mayoral, and Fco. Javier Vilchez. The ADRENALINE testbed: An SDN/NFV packet/optical transport network and edge/core cloud platform for end-to-end 5G and IoT services. In *2017 European Conference on Networks and Communications (EuCNC)*, pages 1–5, 2017.
- [48] Ganesh R Naik and Dinesh K Kumar. An overview of independent component analysis and its applications. *Informatika*, 35(1), 2011.
- [49] Ning Han, SungHwan Shon, Jae Hak Chung, and Jae Moung Kim. Spectral correlation based signal detection method for spectrum sensing in IEEE 802.22 WRAN systems. In *2006 8th International Conference Advanced Communication Technology*, volume 3, pages 6 pp.–1770, 2006.
- [50] Mike Novey and Tulay Adali. Adaptable nonlinearity for complex maximization of nongaussianity and a fixed-point algorithm. In *2006 16th IEEE Signal Processing Society Workshop on Machine Learning for Signal Processing*, pages 79–84, 2006.
- [51] Michael Syskind Pedersen, Jan Larsen, Ulrik Kjems, and Lucas C Parra. Convolutional blind source separation methods. In *Springer Handbook of Speech Processing*, pages 1065–1094. Springer, 2008.
- [52] Sreeraj Rajendran, Vincent Lenders, Wannes Meert, and Sofie Pollin. Crowdsourced wireless spectrum anomaly detection. *IEEE Transactions on Cognitive Communications and Networking*, 6(2):694–703, 2020.
- [53] Dipankar Raychaudhuri, Ivan Seskar, Gil Zussman, Thanasis Korakis, Dan Kilper, Tingjun Chen, Jakub Kolodziejski, Michael Sherman, Zoran Kostic, Xiaoxiong Gu, Harish Krishnaswamy, Sumit Maheshwari, Panagiotis Skrimponis, and Craig Gutterman. Challenge: COSMOS: A city-scale programmable testbed for experimentation with advanced wireless. In *Proceedings of the 26th Annual International Conference on Mobile Computing and Networking, MobiCom '20*, 2020.
- [54] Matías Richart, Javier Baliosian, Joan Serrat, and Juan-Luis Gorricho. Resource slicing in virtual wireless networks: A survey. *IEEE Transactions on Network and Service Management*, 13(3):462–476, 2016.
- [55] Taneli Riihonen, Stefan Werner, and Risto Wichman. Mitigation of loopback self-interference in full-duplex MIMO relays. *IEEE Transactions on Signal Processing*, 59(12):5983–5993, 2011.
- [56] Ashutosh Sabharwal, Philip Schniter, Dongning Guo, Daniel W. Bliss, Sampath Rangarajan, and Risto Wichman. In-band full-duplex wireless: Challenges and opportunities. *IEEE Journal on Selected Areas in Communications*, 32(9):1637–1652, 2014.
- [57] Haiyun Tang. Some physical layer issues of wide-band cognitive radio. *IEEE International Symposium on New Frontiers in Dynamic Spectrum Access Networks 2005*, pages 151–159, 2005.
- [58] TAOGLAS. Specification of the wideband 4G LTE I-Bar antenna, 2017.
- [59] Boston C. Terry, Alex Orange, Neal Patwari, Sneha Kasera, and Jacobus Van Der Merwe. Spectrum monitoring and source separation in powder. In *Proceedings of the 14th International Workshop on Wireless Network Testbeds, Experimental Evaluation & Characterization, WiNTECH'20*, page 25–32, 2020.
- [60] Jie Wang, Boston C. Terry, and Leigh Stoller. Gitlab repository of the proposed full-duplex monitoring system. https://gitlab.flux.utah.edu/Jie_Wang/spectrum-monitor/-/tree/code_merge, 2022.
- [61] Tevfik Yucek and Huseyin Arslan. A survey of spectrum sensing algorithms for cognitive radio applications. *IEEE Communications Surveys Tutorials*, 11(1):116–130, 2009.
- [62] Yonghong Zeng, Ying-Chang Liang, Anh Tuan Hoang, and Rui Zhang. A review on spectrum sensing for cognitive radio: Challenges and solutions. *EURASIP Journal on Advances in Signal Processing*, (1):1–15, 2010.
- [63] Zhongshan Zhang, Keping Long, Athanasios V. Vasilakos, and Lajos Hanzo. Full-duplex wireless communications: Challenges, solutions, and future research directions. *Proceedings of the IEEE*, 104(7):1369–1409, 2016.